ENSO and SAM influence on the generation of long episodes of Rossby Wave Packets during Southern Hemisphere Summer

Iago Pérez[1], Marcelo Barreiro[2], and Cristina Masoller[3]

[1]Departamento de Ciencias de la atmósfera, Facultad de Ciencias, Universidad de la República, Montevideo, Uruguay, [2]Physics deparment-Nonlinear, Universitat Politécnica de Catalunya, Rambla St. Nebridi 22, Terrasa 08222, Barcelona, Spain

Corresponding author: Iago Pérez (iperez@fisica.edu.uy)

Key Points:

- Occurrence of long-lived Wave Packets shows large interannual variability in southern hemisphere summer.
- El Niño and negative Souterhn Annual Mode phases create atmospheric conditions that favor long-lived Rossby Wave Packets.
- Years with largest numbers of long-lived Rossby Wave Packets present a zonally symmetric and narrow upper level jet shifted northward.

Abstract

This study aims at understanding the impact of low-frequency climate modes on Rossby Wave Packets (RWPs) during the southern hemisphere summer. In particular, we focus on long-lived RWPs (lifespan above 8 days) and determine how El Niño-Southern Oscillation (ENSO) and Southern Annular Mode (SAM) modulate their frequency of occurrence plus the main areas of detection and dissipation. We find that the occurrence of long lived RWPs is maximum during El Niño years and negative SAM events. Years with largest numbers of long-lived RWPs are characterized by a zonally symmetric and narrow upper level jet that is shifted northward from its climatological position. Conversely, when the jet is shifted southward, as during positive SAM phases, particularly in the southwestern Pacific basin, the number of long-lived RWPs detected diminishes. El Niño sets atmospheric conditions that support the formation of long lived RWPs whereas La Niña years presents high interannual variability in the frequency of occurrence. Moreover, during El Niño events the main formation area is between 61-120ºE and its main dissipation area between 300-359ºE. During La Niña events, the main formation area moves to 241-300ºE and no main dissipation area is identified. During positive SAM two main formation areas appear at 61-120ºE and 241-300ºE and two main dissipation areas between 121-180º and 301-359º, whereas in negative SAM only one formation area at 241-300º is detected and no main dissipation area is found.

Keywords: long-lived RWPs, ENSO,SAM.

1 Introduction

Atmospheric circulation in mid-latitudes is dominated by the upper level jet and associated storm track. Predictability on time scales longer than the synoptic is limited and on seasonal time scales is directly dependent on tropical surface ocean conditions. On intermediate, subseasonal scales predictability relies on persistent structures such as blockings or Rossby Wave Packets (RWPs).

RWPs are packets of upper-level atmospheric waves that are able to travel coherently for several days by downstream development (Chang and Yu 1999; Chang 2000), and transport large quantities of energy. These packets are constantly being created and destroyed in mid-latitudes and most of them survive only for a few days, but under certain conditions these packets can achieve such stability that they live and propagate for several days or even weeks before disappearing (Grazzini and Vitart 2015).

RWPs represent high-amplitude meanderings of the jet stream and thus are related to storm track variability (Souders et al., 2014a). Moreover they have been referred as precursors of extreme climatological events such as heat waves or droughts, (Chang 2005; Obrien and Reeder 2017; Wirth et al., 2018), as well as extratropical cyclone development, (Chang et al 2005; Sagarra and Barreiro 2019). Additionally, Souders et al., (2014b) remarked that if they are not well represented in models, RWPs can also affect the weather forecasts in the areas they cross, increasing the uncertainty on short and middle range forecasting. Increasing our understanding of processes that control RWPs is thus crucial to understand the mechanisms that governs weather and climate in mid-latitudes, and provides the possibility of extending the forecast beyond synoptic time scales (Grazzini and Vitart 2015).

As mentioned before, under certain conditions RWPs can maintain their coherence longer than usual and are able to survive for weeks in the atmosphere. The lifespan, extension and propagation of RWPs are highly dependent on the potential vorticity gradient and the distribution of adiabatic heating sources (Grazzini and Vitart 2015). Potential vorticity (PV) gradients controls the strength and position of the waveguide where the RWP propagates (Hoskins and Ambrizzi, 1993) in such a way that a very intense and narrow gradient of PV favors the development of coherent RWPs that will last longer in the atmosphere before they disappear (Chang and Yu 1999; Souders et al., 2014b) while weaker gradients tend to stop or damp wave propagation (Grazini and Vitart 2015). RWPs are more easily detected in the Southern hemisphere due to the presence of baroclinically unfavorable continental areas (Grazzini and Vitart 2015). Moreover, during summertime the storm track is almost zonally symmetrical at 50ºS, favoring the propagation of packets (Chang 1999).

RWPs have been extensively studied in recent years in the northern hemisphere (NH). However in the southern hemisphere (SH) there are fewer studies and mainly focused on climatological statistics. Their interannual variability and the influence of global climate modes have not been addressed in detail. Here we will study the impact of El Niño-Southern Oscillation (ENSO) and the Southern Annular Mode (SAM) on the characteristics of RWPs during summertime. It is well know that these climate modes alter the large scale mid-latitude flow and therefore the waveguide where the RWPs propagate. Moreover, we will focus on long-lived RWPs, that is, those packets that live longer than 8 days (Grazzini and Lucarini 2010). Due to their link with extreme climatological evens, the study of long-lived RWPs and their areas of formation/detection may contribute to the improvement of extended range forecasting of extreme events (Grazzini 2007; Wirth et al 2018). Next we describe the main results found in the literature about for RWPs in the SH.

Chang (1999) first describes the properties of upper level wave packets by means of time-lagged one point correlation maps of the meridional velocity. He found that wave packets tend to propagate along the mid-latitude jets and that their zonal group velocity in the SH summer is about 20-25 m/s. Chang (2000) showed that most wave packets propagate dominated by downstream development, and that a surface cyclone developed in nearly all cases to the east of the upper-level troughs associated with the wave packets.

Souders et al., (2014b) found that in the SH, RWPs have a mean lifetime of 7.9 days and travelled a mean of 151 degrees. In contrast, during NH summer RWPs last for about 6 days and travel only 119 degrees. Additionally, RWPs activity in the SH does not show a strong seasonal cycle and the packets detected are faster and more coherent than in the NH. They also found a positive trend in the annual mean activity of RWPs that they hypothesize may be related to an improvement of the quality of the reanalysis (see e.g Barreiro et al 2014) or to the observed trend in the SAM during summer.

Barreiro (2017) studied the interannual variability of wave activity during summertime in the southeast Pacific-Atlantic sector and found that the leading pattern of variability in this region is correlated with ENSO such that there is an increase in transient wave energy in the Pacific during El Niño years. However, this study did not address the characteristics of RWPs.

Sagarra and Barreiro (2020) performed a climatological study of RWPs during the austral summer in the SH. They found a mean of 32 packets per season, 90% of the trajectories have a lifespan of 3-8 days and only 2% above 14 days. In addition 80% of the waves propagated between 30-170º degrees of longitude and only 2% surpasses 360 degrees with a median of 107º. No main area of dissipation/formation on seasonal or monthly time scales was detected. The study did not find a relation between the interannual count of RWPs and the ENSO, but suggested a possible relationship with the SAM (Southern Annular Mode).

In this study we use a similar methodology as in Sagarra and Barreiro (2020) but, as mentioned above, focus on the impact of ENSO and SAM on the RWPs whose lifespan is longer than 8 days.

The manuscript is organized as follows. Chapter 2 describes the data and the algorithm used. Chapter 3 describes the climatology and interannual variability of RWPs as well as the impact of ENSO and SAM on long-lived packets. Lastly Chapter 4 provides a summary of the results.

2. Data and methods

2.1Data

To track RWPs we use daily mean meridional winds (m/s) at 300 hPa as done previously by several authors (e.g. Chang and Yu 1999; Sagarra and Barreiro 2019). This data comes from

NCEP/DOE Reanalysis 2 (NOAA/OAR/ESRL) available in http://www.esrl.noaa.gov/psd/ (Kanamitsu et al., 2002) with an horizontal spatial resolution of 2.5x2.5º. The period of study chosen is the austral summer here considered as December, January,February and March (DJFM) from 1 December of 1979 to 31 March of 2020, retaining data corresponding to 41 summer seasons. After substracting the daily climatology we calculated the amplitude of the wave packet envelope (m/s) using the method of Zimin et al., (2003) retaining wave numbers between 4 and 11 which are representative of the atmospheric transients in the SH (Trenberth 1981). For the methodology of Zimin et al., (2003) to work well the propagation of RWPs has to be in the zonal direction (e.g. Zimin et al., 2006), which is the case for the SH summer as shown by Chang (1999). This latter study also showed that the jet and maximum variance in meridional wind anomalies are in a band centered at 50ºS, and therefore in our study we averaged latitudinally data in the band 40ºS-65ºS.

To characterize the interannual occurrence of the global climate modes we considered the ONI index (Oscillation Niño Index) in the case of ENSO and the AAO index (Antartic Oscillation) for SAM, both datasets available in the NOAA website https://origin.cpc.ncep.noaa.gov/. Of the 41 seasons considered 25 correspond to positive SAM and 16 to negative SAM, which is consistent with the observed positive trend towards positive phases in SAM since the mid-90s. In the case of ENSO, 14 years are classified as “El Niño”, 13 years as “La Niña” and 14 years as Neutral events. We also used geopotential height at 300 hPa (Z300) from NCEP/DOE Reanalysis 2 and sea surface temperature (SST) from the ERSSTv5 dataset (Huang et al., 2017) to study the upper level circulation anomalies and surface ocean conditions, respectively associated with the interannual variability in the occurrence of RWPs.

Finally, to characterize changes in the position and intensity of the waveguide we calculated the meridional gradient of the absolute vorticity (AV) that can be used as an approximation of the isentropic gradients of potential vorticity (Wirth et al., 2018). This was done using 300hPa meridional and zonal monthly mean winds from the NCEP/DOE 2 Reanalysis.

2.2 Methodology

2.2.1 Tracking algorithm

Previously to the application of the algorithm to track RWPs, it is necessary to set a minimum threshold for the amplitude of the envelope to avoid tracking noise**.** However the value of this threshold is not well-defined due to the lack of intrinsic physical properties that distinguish one packet from another (Souders et al., 2014b). As a result, a low threshold tracks noise and a large one will miss information. Grazzini and Vitart (2015) considered a threshold value of 16 m/s, Souders et al., (2014b) 14 m/s and Sagarra and Barreiro (2020) 15 m/s. In this study we considered a threshold of 15 m/s in the calibration of the algorithm and then we analysed the robustness of our findings by considering higher and lower threshold values of 13, 15 and 17 m/s.

The algorithm tracks the amplitude of the envelope above the chosen threshold allowing to follow the trajectory of a coherent wave packet in its trajectory (Grazzini and Vitart 2015; Sagarra and Barreiro 2020). The algorithm consists of following steps:

1.-Detect of the highest value of the amplitude in the longitudinal axis (p_n) in the first day of the data matrix.

2.- Search for the position of the maximum amplitude eastwards the next day (p_{n+1})

3.-If the points p_n and p_{n+1} are between [p_n+15º to p_n+45º], p_n and p_{n+1} are registered as part of the same trajectory and we repeat steps 2 and 3 for the following days. The distance is chosen so that the wave packet travels at a speed between 15-45º per day as found in the literature (Sagarra and Barreiro 2020).

4.- When we find a maximum p_m that it is not within the range specified in step 3 or when we reach the limit of the data matrix, the trajectory is saved and we resume the tracking from the last day we detected the start of a trajectory.

5.-After analyzing all longitudes for the day, we proceed to the next one and repeat steps 1-4 until we analysed the whole data matrix.

6.-After finishing the analysis of the data matrix we check for trajectories that may have been truncated and apply proximity criteria shown in Table 1 to link them. That is if two trajectories are closer than 1000 km and their difference in slope are less than 20º/day they are joined. Additionally, for slow trajectories that were separated by 1-2 days but the mean speed between the end of a trajectory and the start of the next one is less than 15º/day, they were considered as a single trajectory if the mean speed between points L-1 or L (being L the last point of the first trajectory) to I or I+1 (being I the initial point of the second trajectory) is 15º/day or above and fulfilled the rest of the conditions set in Table 1.

7.-Finally, we filtered out trajectories with a duration shorter than three days because they are not relevant to this study.

Minimum threshold	15 m/s
Distance	1000 km
Slopes differences	20º/day
Mean speed per day	[15-45 º/day]
Days separated	1-2 days

Table 1: Proximity criteria used in the tracking algorithm

After running the algorithm, we performed a statistical analysis of the RWPs detected. The following measures are considered: (i) mean propagation speed (m/s) taking into consideration that 1º/day is approximately 0.82 m/s in the latitudinal region analysed (40-65ºS) , (ii) duration (days during which a trajectory can be tracked until it disappears), (iii) length of the trajectory extension (difference between the starting and ending point of the trajectory) in degrees and (iv) areas of formation and dissipation, being formation the area where the RWPs surpasses the minimum envelope threshold so the packet is sufficiently coherent to be tracked and dissipation the last point recorded of the trajectory. Then, we studied the interannual variability of wave packets and the impact of global climate modes.

2.2.2 Classification of the identified trajectories

RWPs are classified into three categories based on their lifespan: short-lived RWPs (SL) if their lifespan ranges between 3-6 days, medium-lived RWPs (ML) when their lifetime ranges between 7-8 days and long-lived RWPs (LL) when they last more than 8 days. Although this study is focused on long-lived packets we also registered RWPs of different lifespans to study whether their frequency of occurrence is correlated. As pointed out above we considered several thresholds and as expected we found a decreasing number of LL RWPs with increasing threshold, so that for 17m/s the algorithm detects very few RWPs.

2.2.3 Identification of the formation and dissipation areas and correlation with ENSO and SAM events.

To study the formation and dissipation areas we considered the following 6 regions in order to condense the information: 0-60ºE,61-120ºE,121-180ºE,181-240ºE,241-300ºE and 301-359ºE.

A linear regression and correlation analysis between the time series of interannual occurrence of RWPs with Z300 and SST anomalies was conducted. This allows to determine the large scale circulation anomalies and oceanic conditions that accompany changes in the frequency of occurrence of RWPs, which may be in turn related to ENSO and SAM. The statistical significance of the result is assessed using a student t- test at 10 % significance level.

We also constructed composite maps considering the four years with largest and smallest frequency of occurrence of long-lived RWPs using a threshold of 15 m/s. We plotted the upper-level zonal winds and the meridional gradient of absolute vorticity in order to study the main changes in the structure and intensity of the waveguide. To complement the analysis composite maps were also constructed separately during El Niño and La Niña years as well as during positive/negative SAM events using only three years per event in these cases due to the short record available. Lastly we also performed one point lag linear regression maps between days -4 and +6 of the RWP amplitude to illustrate changes in the propagation under different conditions.

3. Results

3.1 Mean and interannual variability of RWPs

Before applying the algorithm, we calculated the climatological amplitude of the envelope in the SH. The highest values of the amplitude are located in the latitudinal band between 40-60ºS and from 50-250 º E (Figure 1). There is a minimum located around the southern tip of South America consistent with the results of Souders et al., (2014a) (in their case on annual time scale). The spatial structure is similar on individual months (not shown). As a result RWPs tracked using restrictive thresholds could be abruptly interrupted in this area and may cause the detection of high dissipation rates between 280-330ºE.

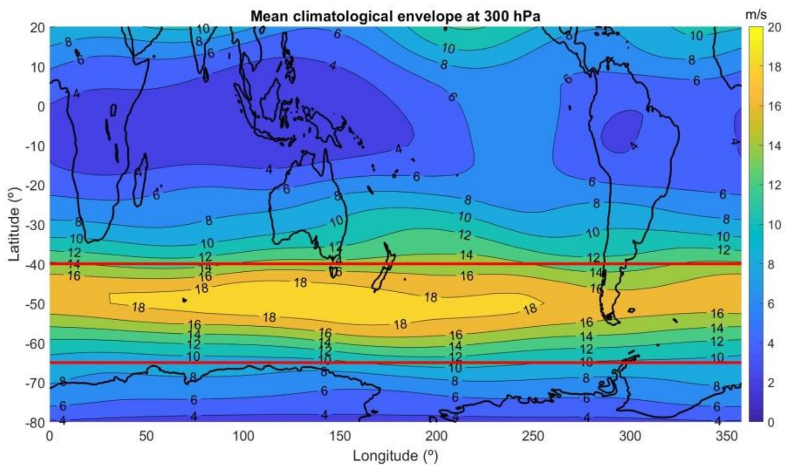

Figure 1. Mean climatological amplitude (m/s) during DJFM solid red lines shows the limitations of the area of study.

Figure 2 presents a summary of statistics of RWPs properties. It shows an exponential decrease in the duration of the wave packets such that about 70% do not reach 7 days and barely 2% of the trajectories have a lifespan of 14 days or above during the season. In addition, Figure 2 shows that around 80% of the trajectories travel between 30º-170º in the longitudinal direction and only about 2.5% are able to go around the globe. The mean distance travelled by a packet is 128 º, the median is 84º and the inter-quartile is 85º. In the case of the waves' lifespan they show a mean duration of 5 days, a median of 4 days and an inter-quartile range of 3 days. These results are close to those obtained by Sagarra and Barreiro (2020). Also Sagarra and Barreiro (2020) found that the mean speed of the packets is 20 m/s with a standard deviation of 6,6 m/s, while in our study we have obtained a mean speed of 21 m/s and a standar deviation of 4.3 m/s. The mean duration found here is lower than in Souders et al., (2014b), which may be, at least partially due to the use of a less restrictive threshold in that study (14 m/s).

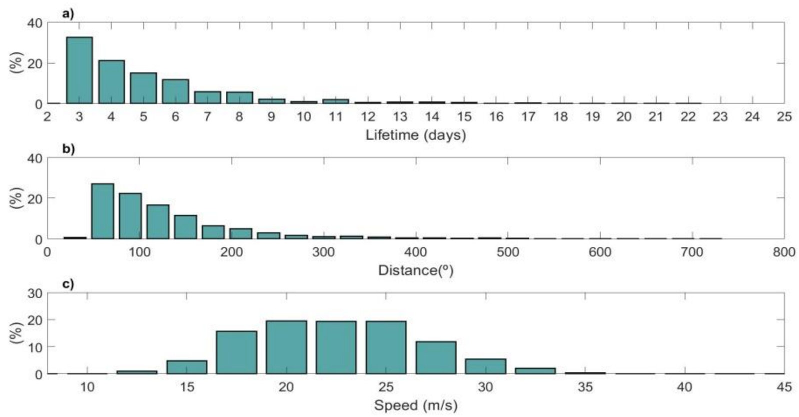

Figure 2. Climatological properties of RWPs tracked between 1979-2020 during DJFM using a minimum threshold of 15m/s; (a) lifespan, of RWPs (b) distance travelled, and (c) the mean speed per packet.

The frequency of occurrence of the total number of RWPs shows large interannual variability, such that there are years with a minimum of 20 and years with a maximum of 40 events (Figure 3a). In addition the time series of RWPs detected are highly correlated for different thresholds, but the number diminishes significantly for 17m/s. Looking at subsets of RWPs, it is clear that the overal behaviour of the total number of events is dominated by the variability in occurrence of SL waves. For ML and LL waves the number of events per year is similar, relatively small and sensitive to the threshold used so that their number increases with a lower threshold. In contrast, they show large interannual variability percentage wise, suggesting that large scale circulation conditions set up by low-frequency climate modes can modulate their occurrence.

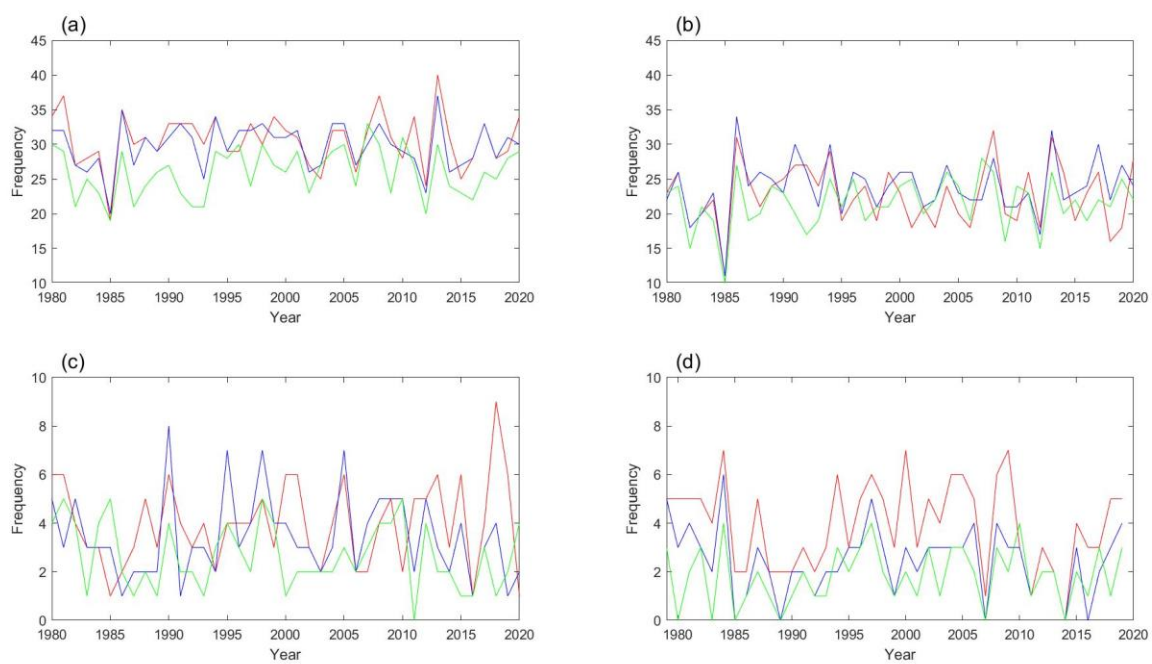

Figure 3. Interannual variability of the total RWPs tracked (a), short-lived waves (b), medium-lived waves (c), and long-lived waves (d). Red blue and green lines indicate the results obtained using thresholds of 13,15 and 17 m/s, respectively.

In the next section we study this focusing on the LL RWPs, given that a better understanding can provide maximum improvements on prediction on long-range to subseasonal scales. It is also worth mentioning that there is a negative correlation between the occurrence of SL and LL waves with r=-0.47 for a threshold of 15 m/s, so that the detection of several LL waves also mean less SL waves during that particular year. This correlation value is statistically significant according the t student test with a 90% of significance.

3.2 Impact of SAM and ENSO on long-lived packets

Figure 4 shows the frequency of occurence of the total number of RWPs stratified according to the different phases of ENSO and SAM. In the case of SAM, both phases show a similar median for thresholds of 13 and 15 m/s, while a positive phase favours the occurrence of RWPs against negative SAM for a threshold of 17 m/s. This latter result is in agreement with Sagarra and Barreiro (2020). In the case of ENSO, El Niño and La Niña events present less RWPs than Neutral years for thresholds of 13 and 15 m/s while for a threshold of 17 m/s El Niño events tends to favour more RWPs than during La Niña. Similar results are found considering only SL waves, consistent with the fact that they represent the largest percentage of waves.

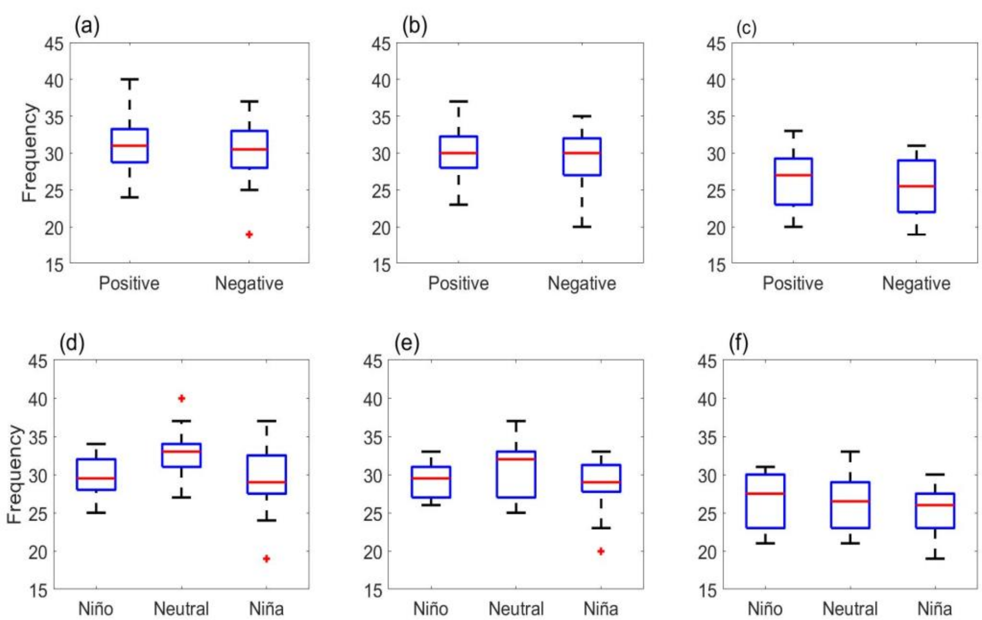

Figure 4. Boxplots of interannual variability of all RWPs detected during different SAM (a-c) and ENSO (d-f) phases for different minimum thresholds.

When we focus on long-lived RWPs, the algorithm detected a larger number of waves during El Niño compared to Neutral and La Niña years, particularly for a threshold of 13 m/s, although the result holds for other thresholds as well (Figure 5a). Additionally the dispersion of LL RWPs detected during El Niño is lower compared to Neutral and La Niña years. During La Niña years the frequency of occurerence of RWPs shows much higher interannual variability than during El Niño events for the lowest threshold.

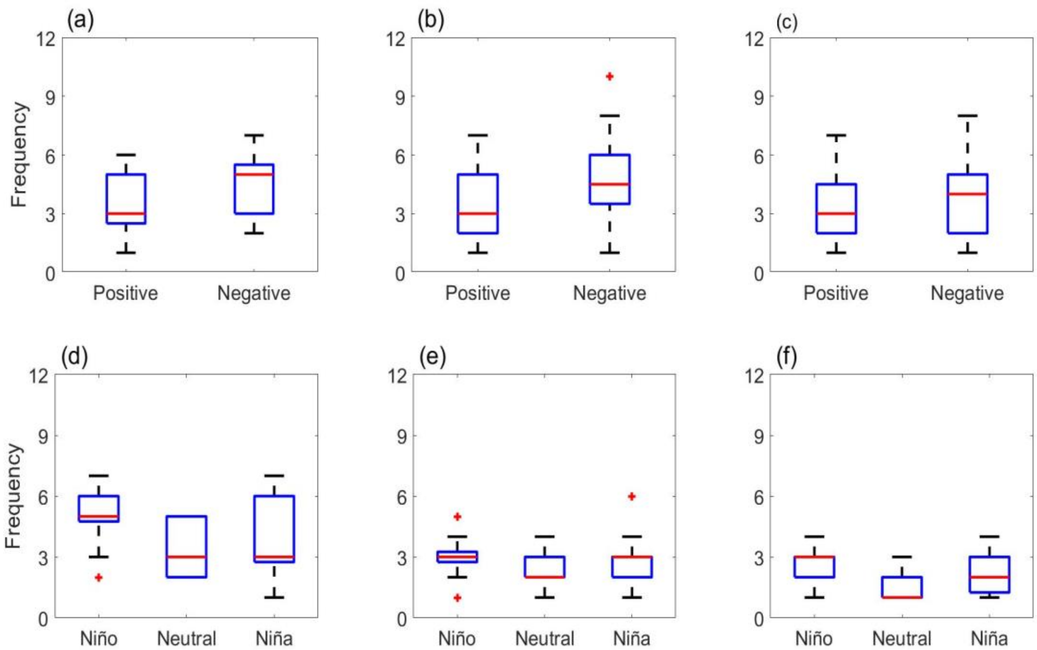

Figure 5. Analogous to figure 4, but for long-lived RWPs.

ENSO also affects the formation and dissipation areas of LL RWPs (Figure 6). During El Niño events, there is a main formation area between 61-120ºE (South-Southwest of Australia) and a secondary area at 241-300ºE (East of South America), whereas in the case of La Niña only the latter is a well defined formation region. On the other hand, during El Niño events there is a main area of dissipation in the South Atlantic (301-359ºE) while in the case of La Niña no region stands out. These results are independent of the threshold considered. Note that in the case of El Niño there seems to be a compensation in detection of LL RWPs in the regions (0-60ºE) and (61-120ºE), depending on the threshold. For example, similar number of LL RWPs are detected in these two areas for 13 m/s, but for 17 m/s the number detected is much larger in (61-120ºE) than (0-60ºE). A plausible explanation is that most of the waves detected in the 0-60ºE secion using the lowest threshold are spotted in the following area when we applied more restrictive thresholds becase the packet amplitude had more time to grow.

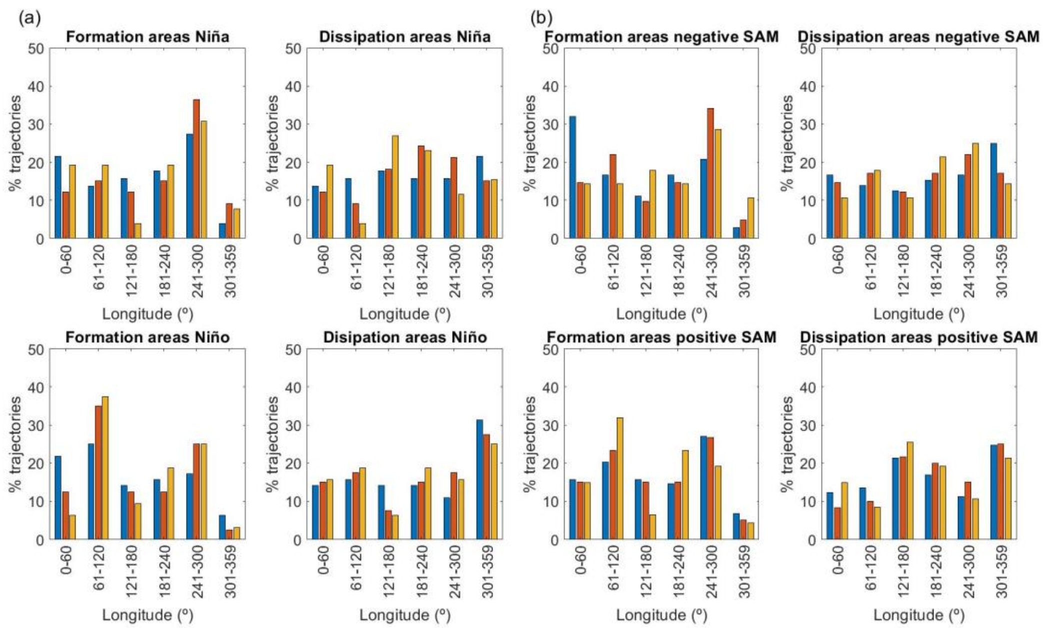

Figure 6. Formation and dissipation areas found during el Niño and la Niña events (a), and during positive and negative SAM (b). Colorbars represent different minimum thresholds, being the blue 13 m/s, orange 15 m/s and yellow 17 m/s.

Regarding the impact of SAM (Figure 5b), we observe that independently of the threshold, negative SAM conditions favour the detection of LL RWPs. Both phases have large dispersion but the median is always higher in the negative phase, especially for the lowest threshold (13 m/s) which statistics is more robust due to the higher number of cases. As for main areas of formation, during positive SAM, the main formation regions are located in the eastern Pacific (241-300ºE) and over South-Southeastern Africa (61-120ºE). During negative SAM phases only the region located in the eastern Pacific stands out for all thresholds (Figure 6). In the case of dissipation there are two main areas in positive SAM: over the South Atlantic basin (301-359ºE) and to the Southwest of Australia (121-180ºE), where about 50% of the LL RWPs are no longer detected. On the other hand, in the case of negative SAM there is no main area of dissipation consistent for all thresholds.

According to above results, LLRWPs are influenced by both ENSO and SAM, in such a way that there is an increase in the frequency of the occurrence during El Niño and negative SAM phases. This influence can be seen in the regression maps of sea surface temperature and 300hPa geopotential height anomalies against the (standarized) time series of occurrence of LL RWPs (Figure 7). Results are shown for a threshold of 13 m/s because the number of LL RWPs is larger and the statistics are more robust, (nonetheless the patterns for a threshold of 15 m/s are very similar but with weaker anomalies). As expected from the boxplots an increase in the number of detected LL RWPs is correlated with positive tropical Pacific sea surface temperature anomalies (Figure 7a). Moreover it is correlated positively with the southeaster Pacific and negatively with the southwestern Atlantic.

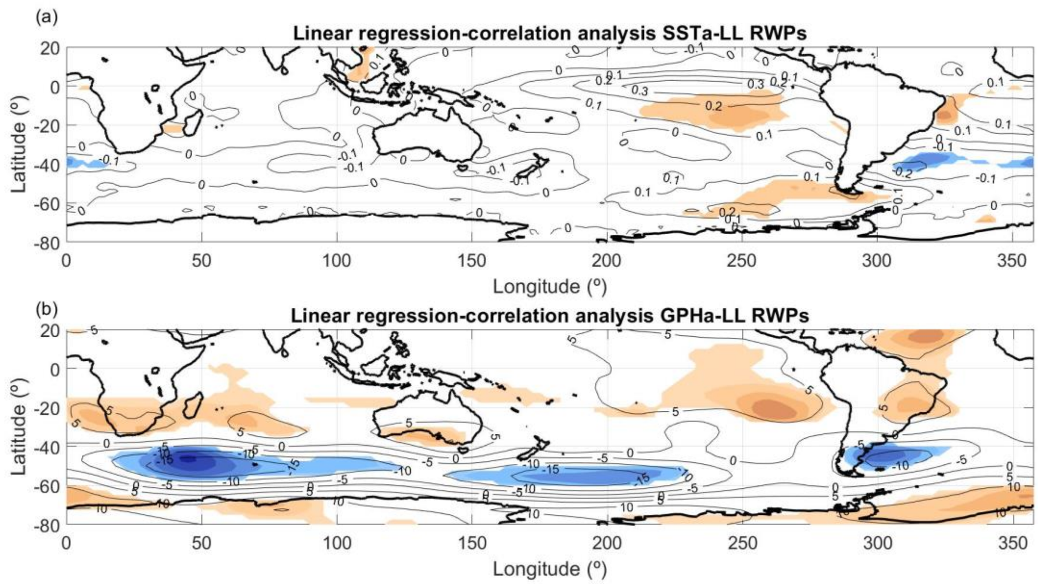

Figure 7. Linear regression maps of SST anomaly (above) and 300hPa GPH anomaly (down) with respect to the time series of LL RWPs for a threshold of 13 m/s. The colored areas indicate where the correlation is significant at the 10% level and black lines the value of linear regression.

Consistent with these results, the tropical upper level geopotential height shows positive anomalies during years of increased LL RWPs (Figure 7b). In addition, there is a decrease in Z300 in midlatitudes and an increase in high latitudes, signalling the occurrence of the negative phase of SAM. Thus this map is in agreement with the results of Figure 5 and suggests that the jet and by extension, the waveguide, are enhanced and shifted northward during years of increased LL RWPs. In the next section we describe in more detail the changes in the jet.

3.3 Modification of the waveguide

Figure 8 shows a composite map of the upper level zonal winds and meridional gradient of absolute vorticity (GAV) constructed for the four years with the most and least number of LL RWPs detected for low (13 m/s) and medium (15 m/s) thresholds. We observe that the jet and the waveguide are more zonally symmetric during years of maximum number of LL RWPs. Moreover during the years with the smallest number of LL RWPs detected using a low threshold (13 m/s, Figure 8b) the jet and the waveguide are displaced southward, particularly between 130-220ºE, compared with years with the highest occurrence of LL RWPs, (Figure 8a). Similar results are found using a medium threshold (15 m/s, Figures 8c, 8d). This is further illustrated in Figure 9 which show the difference of the zonal mean winds and GAV between years of maximum and minimum detection of LL RWPs for both thresholds.

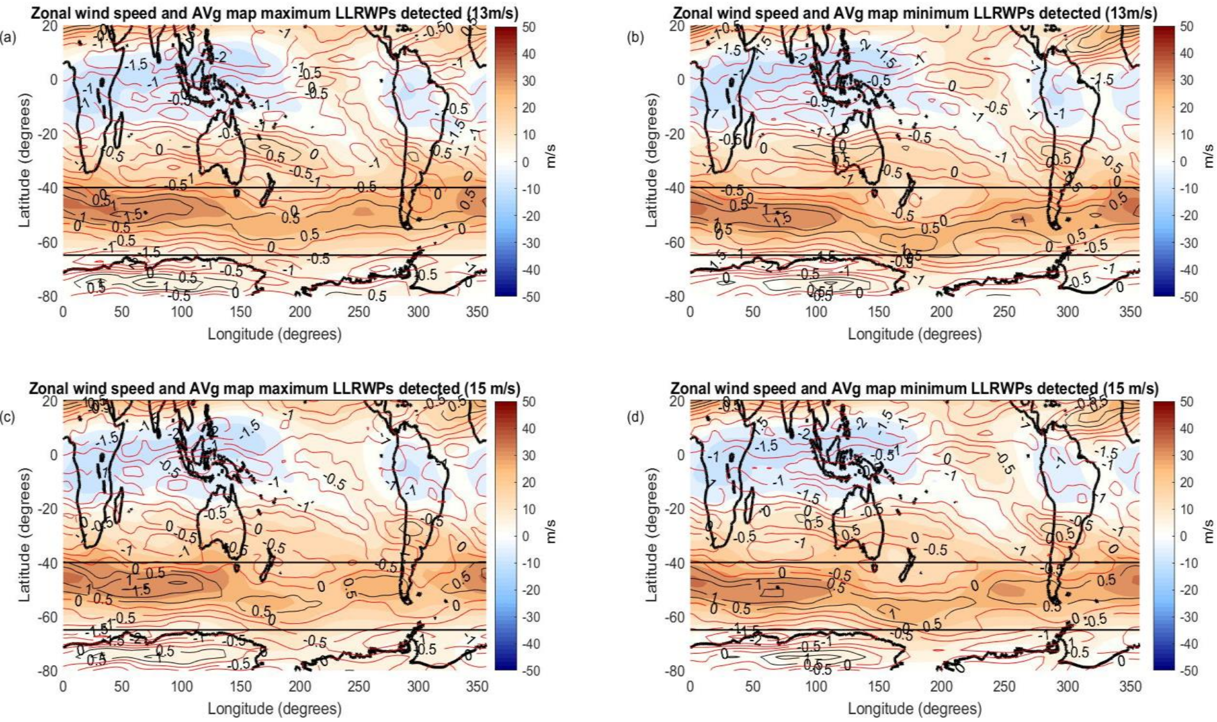

Figure 8. Mean zonal wind and meridional absolute vorticity gradient (AVG) during the 4 years with maximum (a, c) and minimum(b, d) number of LL RWPs detected for thresholds of 13m/s (upper row) and 15 m/s (down row). Zonal wind speed (m/s) is indicated in the colorbar while GAV is represented with black (positive values) and red curve lines (negative values). The units of the AV gradient (1/ms) are multiplied by a factor of 10^{10} to enable an easier visual representation. Red straight lines limit the area of study.

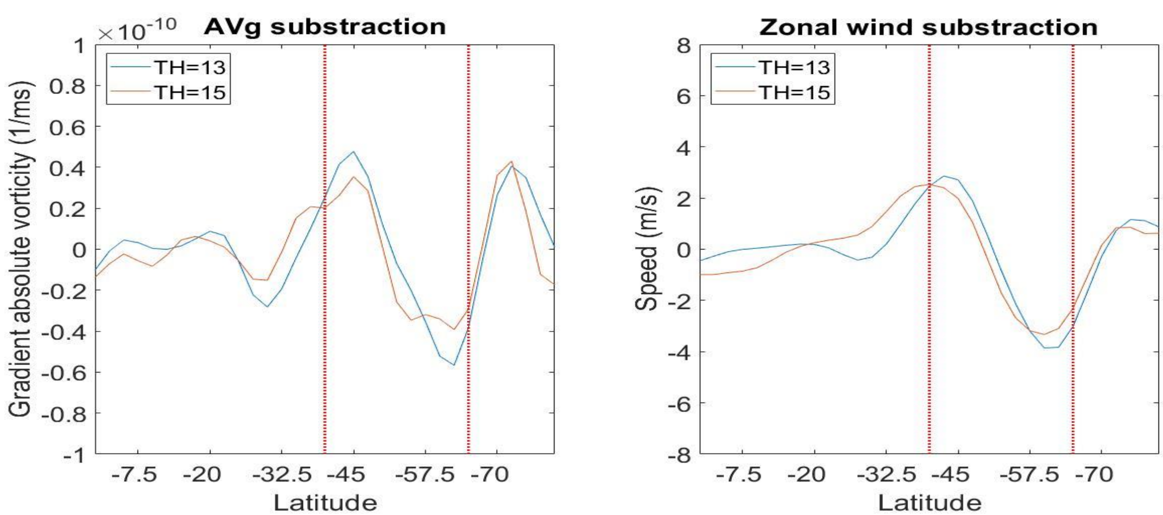

Figure 9. Difference of the zonal mean AV gradient (left) and zonal wind speed (right) between years with maximum and minimum number of LL RWPs for thresholds 13m/s (blue) and 15 m/s (orange). Red lines indicate the limits of the area of study (40-65ºS).

To illustrate the differences in the trajectory of wave packets we perform a linear regression of the wave packet amplitude with respect to that of a point located in 200ºE,50ºS from lag -4 to lag +6 (Figure 10). This location is chosen because it is in the middle of the Pacific sector where the largest differences in the zonal winds between extreme cases of RWPs was found. The maps show that the RWPs show largest amplitudes and are more coherent during the 11 days for the years with the largest number of LL RWPs detected, particularly on lags -2, +2 and +4. At lag +6 it is still possible to capture the propagation of the packet in the case of maximum number of LL packets, whereas for years with the least packets the regression does not show a consistent area. This result further supports the hypothesis that the northward deviation of the mid-latitude jet favours the propagation of LL RWPs, as shown above.

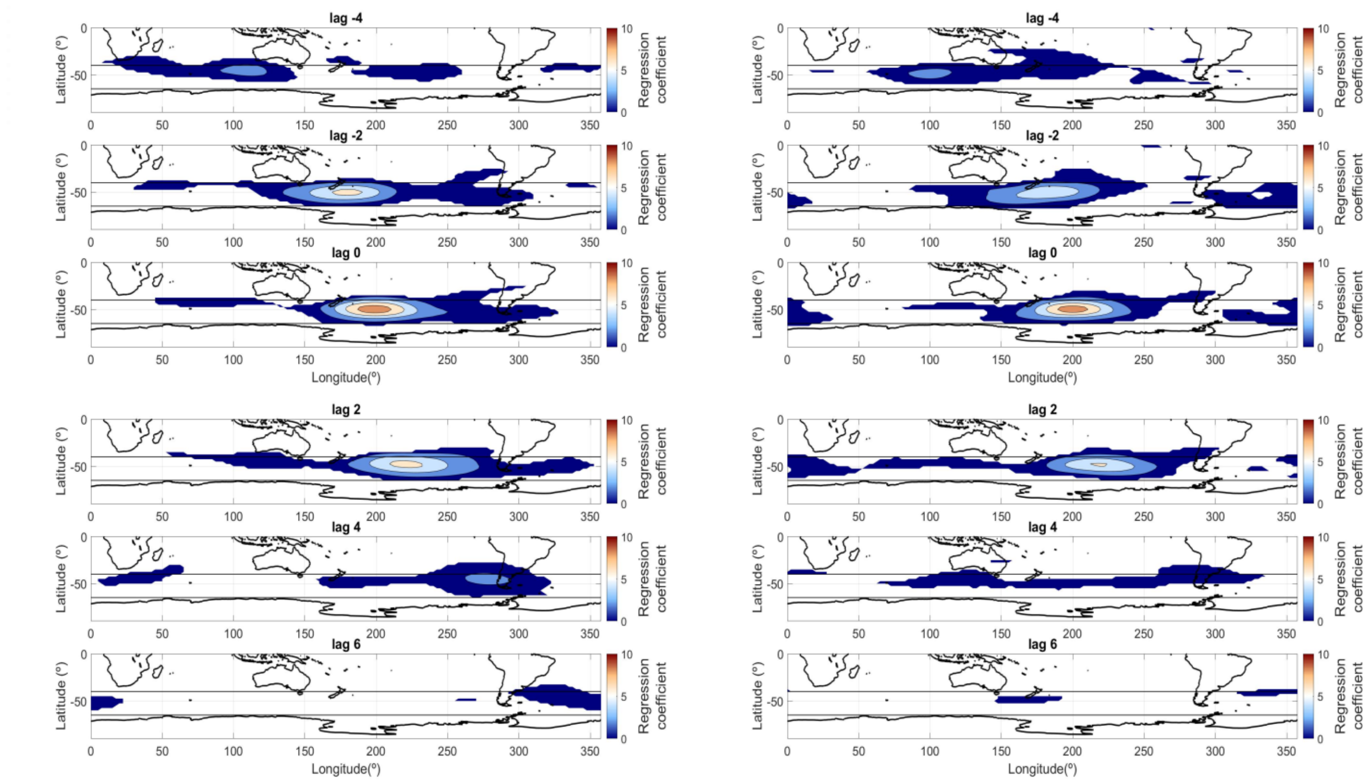

Figure 10. Lag linear regression maps of the envelope amplitude with respect to that of a point located in the middle of the Pacific basin in 50ºS 200ºE during the years of maximum (left) and minimum (right) frequency of LL RWPs.

We now assess changes in the jet associated with the phases of SAM in more detail. To do so we compare the most extreme three years of positive and negative SAM phases (Figure 11). As expected, during the positive SAM phase the jet stream is located further south compared to the negative SAM phase. Moreover, during the negative SAM the jet is zonally symmetric between the south Atlantic and the south of Australia (250ºE and 150ºE) and weak in the Pacific sector, interrupting the waveguide. On the contrary, during SAM positive phase the jet is overall stronger, but it has a more diagonal structure particularly in the Indian-Pacific sector that does not favour the zonal propagation of wave packets. Consistently this shape is similar to the one observed during the years of minimum number of LL RWPs (see e.g. Figure 8b).

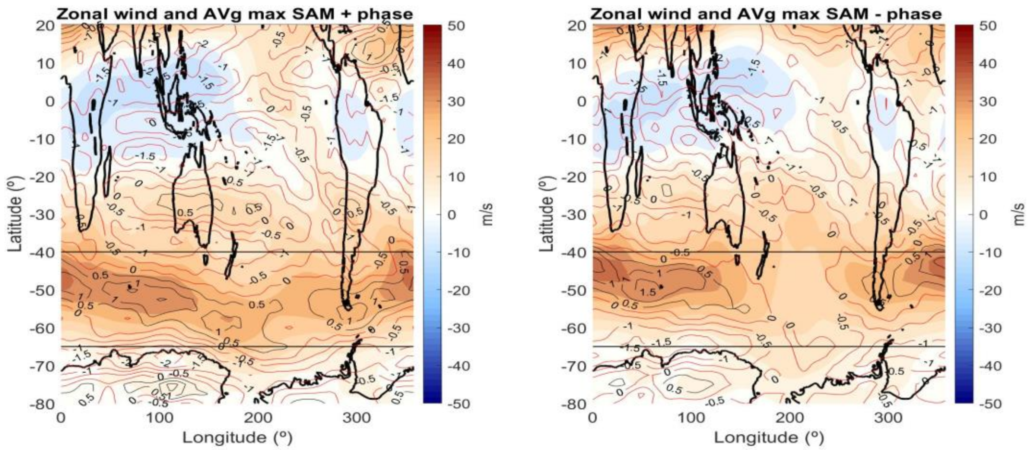

Figure 11. Mean zonal wind and meridional absolute vorticity gradient (GAV) during the 3 years with maximum positive (left) and negative (right) SAM phases. Zonal wind speed (m/s) is indicated in the colorbar, while the GAV is represented with black (positive value) and red lines (negative values). The units of the AV gradient are multiplied by a factor of 10^{10}/ms to enable an easier visual representation.

The importance of a zonally symmetric shape of the waveguide in favouring the detection of RWPs can be further shown comparing the flow during years with maximum number of LL RWPs detected during El Niño and La Niña events (for a threshold of 13 m/s) in Figure 12. In both cases we detected the same number of RWPs (6-7 per year) and the jet is both zonal and narrow. Nonetheless, it can be seen that during La Niña the jet begins to the Southwest of Chile and ends to the south of Australia, whereas during El Niño years it begins in the South Atlantic basin ending to the south of New Zealand. Thus, a high number of LL RWPs develop in a zonal and narrow flow independently on the longitudinal sector it occupies.

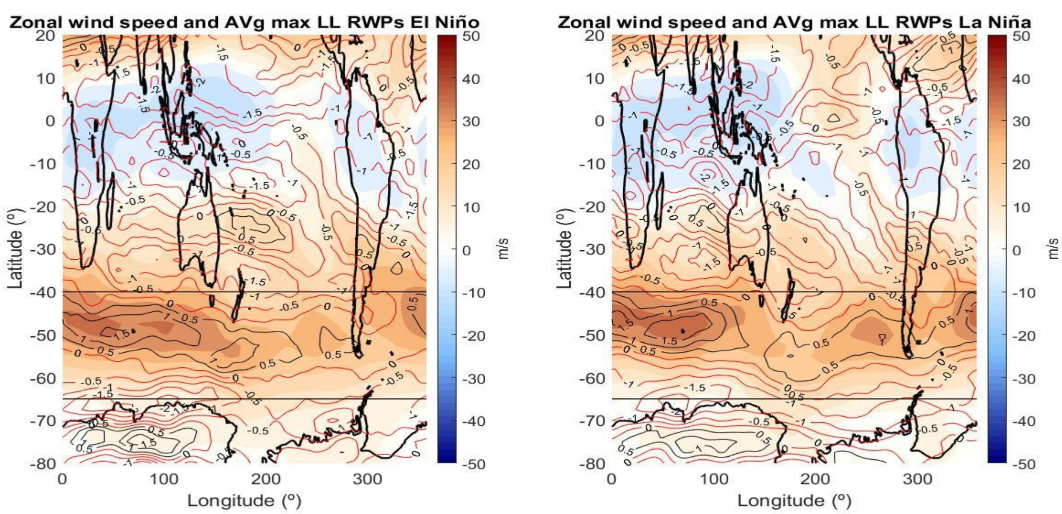

Figure 12. Analogous to Figure 11, but for the years with maximum frequency of LL RWPs during El Niño (left) and La Niña (right) events using the lowest threshold (13 m/s).

4.Summary

A detection algorithm was implemented to study the interannual variability of RWPs, and in particular the impact of SAM and ENSO on those that have a lifespan longer than 8 days.
We have shown that ENSO and SAM control the frequency of occurrence and formation/dissipation areas of LL RWPs, such that El Niño and a negative phase of SAM favour higher numbers. Both conditions favour a more nortward position of the jet stream which is also narrow and more zonally symmetric. Moreover results show that La Niña can also provide background conditions for the occurrence of large number of LL RWPs, but the dispersion is large, suggesting that only a few particular events favour the generation of these long-lived packets.

The formation and dissipation areas of LL RWPs differ depending on the phase of ENSO and in some cases they depend on the threshold considered. In the case of formation areas, during La Niña events it is shown that most of the LL RWPs (near 30%) are detected at the eastern Pacific basin (241-300ºE), which is consistent with the beginning of the jet to the southwest of Chile seen in Figure 12. On the other hand, no main dissipation area was detected. In the case of El Niño, the main formation area is located at 61-120ºE, and the main dissipation area is located at 300-359ºE.

During SAM both phases have the same main formation area as in La Niña events (eastern Pacific 241-300ºE) and positive SAM phases showed another maximum at 61-120ºE (as in El Niño). Thus there are two main formation areas of LL RWPs in the SH, whose importance vary interannually depending of the dominant mode of variability. As in Niño events, the main dissipation area for positive SAM occurs in the south Atlantic possibly associated with the minimum in envelope amplitude seen in Figure 1.

Results found in this study thus suggest that LL RWPs are more common during years with El Niño and negative SAM phases. Given their link with extreme weather events, our results are indicative that extended range forecasting of extreme events may be more feasible during years when the global modes of climate variability are present in these phases, and will be less skilful when La Niña and positive SAM phases are present.

Acknowledgements

This project has received funding from the European Union’s Horizon 2020 research and innovation programme under the Marie Skłodowska-Curie grant agreement No 813844 (ITN CAFÉ). C.M acknowledges partial support from Spanish Ministerio de Ciencia,Innovación y Universidades (PGC2018-099442-B-I00) and from ICREA ACADEMIA program of Generalitat de Catalunya.

Data Availability Statement

NCEP/DOE Reanalysis 2 and ERRST v5 can be downloaded at the websites: https://psl.noaa.gov/data/gridded/data.ncep.reanalysis2.html and https://psl.noaa.gov/data/gridded/data.noaa.ersst.v5.html. ENSO and SAM indexes are available at **https://origin.cpc.ncep.noaa.gov/**

References

Barreiro, M., N. Diaz, M. Renom,2014: Role of the global oceans and land-atmosphere interaction on summertime interdecadal variability over northern Argentina *Climate Dynamics*, 42 1733-1753, doi:10.1007/s00382-014-2088-6

Barreiro M, (2017) Interannual variability of extratropical transient wave activity and its influence on rainfall over Uruguay *International Journal of Meteorology*, 37 4261–4274.

Chang, E. K. M ., and D. B. Yu, 1999:Characteristics of wave packets in the upper troposphere. Part I:Northern Hemisphere winter. *Jorunal of Atmospheric Sciences*, 56(11), 1708-1728,doi: https://doi.org/10.1175/1520-0469(1999)056<1708:COWPIT>2.0.CO;2

Chang, E. K. M., 1999:Characteristics of wave packets in the upper troposphere. Part II: Seasonal and hemispheric variations. *Jorunal of Atmospheric Sciences*, 56(11), 1729-1747. https://doi.org/10.1175/15200469(1999)056<1729:COWPIT>2.0.CO;2

Chang, E. K.M., 2000:Wave Packets and Life Cycles of Troughs in the Upper Troposphere: Examples from the SouthernHemisphere, Summer Season of 1984/1985 *Monthly Weather Review*, 128(1), 25-50.

Chang, E. K.M., 2005 The Impact of Wave Packets Propagating across Asia on Pacific Cyclone Development, *Monthly Weathe Review*, 133(7), 1998-2015

Grazzini, F and Vitart F. 2015 Atmospheric predictability and Rossby wave packets. *International Journal. of the Royal . Meteorological. Society*, 141(692), 2793-2802

Grazzini F, Lucarini V.2010. Climatology of extratropical atmospheric wave packets in the Northern Hemisphere. Available at https://arxiv.org/abs/1011.3564

Grazzini F. (2007). Predictability of a large–scale flow conducive to extreme precipitation over the western Alps. *Meteorology and Atmospheric Physics*, 95, 123-138

Huang, B., Peter W. Thorne, et. al, 2017: Extended Reconstructed Sea Surface Temperature version 5 (ERSSTv5), Upgrades, validations, and intercomparisons. *Journal of Climate*, 30(20), 8179-8205, doi: 10.1175/JCLI-D-16-0836.1

Hoskins, B,J and Ambrizzi T. 1993, Rossby Wave Propagation on a realistic Longitudinally VaryingFlow. *Journal of Atmospheric Science*, 50(12), 1661-1671

Kanamitsu, M., Ebusuzaki, J.Woollen , S. K. Yang S.-K. Yang, J.J. Hnilo, M. Fiorino, and G.L. Potter. 2002 NCEP-DOE AMIP-II Reanalysis (R-2) *American Meteorology Society*, 83 1631-1644

Karami,K., Braesicke P.,Sinhuber, M, and Versick, S. 2016. On the climatological probability of the vertical propagation of stationary planetary waves, *Atmospheric Chemistry and Physic*, 16 Pág 8447-8460 https://doi.org/10.5194/acp-16-8447-2016

O'Brien L., Reeder J. M; 2017 Southern Hemisphere Summertime Rossby Waves and Weather in the Australian Region. *Quarterly Journal of the Royal Meteorologica Society*, 143 Issue 707 2374-2388.

Sagarra R and Barreiro M. 2018 Characterization of extratropical waves during summer of the

Southern Hemisphere (Meteorologica, available in: http://scholar.googleusercontent.com/scholar?q=cache:QRrfUWEuzccJ:scholar.google.com/+sagarra+and+barreiro+2019+meteorologica&hl=es&as_sdt=0,5).

Souders M. B.Souders, Colle, A. B. and Chang M K D (2014b). A Description and Evaluation of an Automated Approach for Feature-Based Tracking of Rossby Wave Packets. *Monthly Weather Review*, 142(10), 3505-3527

Souders M. B.Souders, Colle, A. B. and Chang M K D (2014) The climatology and characteristics of Rossby Wave Packets using a feature-based tracking technique. *Monthly Weather Review*, 142(10), 3528-3548.

Trenberth E, K; 1981 Observed Southern Hemisphere Eddy Statistics at 500 mb: Frequency and Spatial Dependence *Journal of Atmospheric Science*, 38(12), 2585-2605.

Wirth. V., Riemer M, Chang E,K,M., Martius O. 2018.Rossby Wave Packets on the Midlatitude waveguide- a review. *Monthly Weather Review*, 146(7), 1965-2001.

Zimin V, A; Szunyogh I; Patil, J, D; Hunt . R. B; Ott E., 2003 Extracting envelopes of Rossby Wave Packets *Monthly Weather Review*, 131(5), 1011-1017.

Zimin A, V; Szunyogh I; Hunt R. B; Ott E; 2006 Extracting envelopes of Nonzonally Propagating Rossby Wave Packets. *Monthly Weather Review*, 134(4), 1329-1333.